Supporting Information

High-efficiency Nickel Recovery from Spent Electroless Nickel Plating Solution: Effective Degradation of High-concentration Nickel Complexes to Form Nickel Ferrite Nanomaterial via Fe$_3$O$_4$ Catalytic Oxidation

Kaibin Lu,[ac] Jiemin Qin,[ad] Meihua Hu,[ad] Limeng Hu,[a] Minlin Mao,*[ac] Xiaoqin Li,[ac] Zhang Lin,[b] and Weizhen Liu *[acd]

a. School of Environment and Energy, Guangdong Provincial Key Laboratory of Solid Wastes Pollution Control and Recycling, South China University of Technology, Guangzhou, Guangdong 510006, PR China. E-mail: weizhliu@scut.edu.cn.

b. Chinese National Engineering Research Center for Control & Treatment of Heavy Metal Pollution, School of Metallurgy and Environment, Central South University, Changsha, Hunan 410083, PR China.

c. The Key Laboratory of Pollution Control and Ecosystem Restoration in Industry Clusters (Ministry of Education), Guangzhou, Guangdong 510006, PR China.

d. Guangdong Engineering and Technology Research Center for Environmental Nanomaterials, South China University of Technology, Guangzhou, Guangdong 510006, China

This information contains 9 tables and 14 figures.

Contents

Table S1 The characteristics and quality parameters of spent electroless nickel plating solution

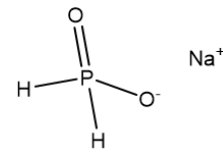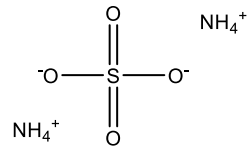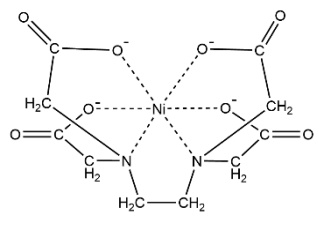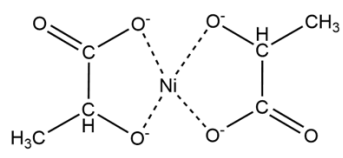| Solution properties	Value
Total Ni	12448.8±1099.4 mg/L
Total P	45032.2±2571.43 mg/L
TOC	23417.5±1631.25 mg/L
$N(NH_3)$	18000±1157.63 mg/L
pH	4.63-5.10
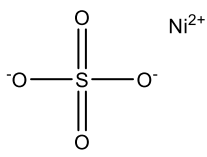
Table S1 exhibited the characteristics and quality parameters of spent electroless nickel plating solution (SENPS), which the concentration of nickel and phosphorus was as high as 12448.8 mg/L and 45032.2 mg/L respectively. Because of organic chelates containing, TOC content of SENPS was about 23417.5 mg/L. Besides, ammonia had a content of about 18000 mg/L in SENPS due to addition of ammonium hydroxide during the electroless plating process.

Table S2 Summary of detection of nickel complexes in spent electroless nickel plating solution by negative ESI mode UPLC-MS

Compound	m/z	Chemical formula	Species	IHD
1	234.9759	$C_6H_{10}NiO_6$	$[M-H]^-$	3
2	350.0193	$C_{10}H_{16}N_2NiO_8$	$[M-H]^-$	5

Table S2 showed the summary of detection of nickel complexes in SENPS by negative ESI mode UPLC-MS containing m/z, chemical formula, species and hydrogen deficiency index (IHD).

Table S3 Chemical composition of spent electroless nickel plating solution

Composition	Formula
Nickel sulfate (NiSO$_4$)	
Sodium hypophosphite (NaH$_2$PO$_2$)	
ammonium sulfate (NH$_4$)$_2$SO$_4$	
EDTA-Ni (C$_{10}$H$_{14}$N$_2$NiO$_8$)	
Nickel lactate ((C$_3$H$_5$O$_3$)$_2$Ni)	

Chemical composition of SENPS was listed in **Table S3**, which the inorganic components NiSO$_4$ and NaH$_2$PO$_2$ were the residue of nickel source and reducing agent in the process of electroless nickel plating. NH$_4^+$ was produced in the waste solution due to the addition of ammonia during the electroless plating process in order to adjust the reaction pH value. The organic components nickel lactate and EDTA-Ni were generated by the chelation of nickel ions and complexing agents adding in the process of electroless plating process, which were analyzed by FTIR (**Fig. S1**) and UPLC-MS (**Fig. 2**).

Table S4 Element analysis of solid product of the reaction (pH=14, 0.1 g/mL Fe$_3$O$_4$, 25 °C, 12 h)

	C	H	O	N	S
Mass (%)	3.16	1.641	22.843	0.00	0.392

It could be seen from **Table S4** that elements C, H, O, N and S in the solid product generated at the condition (pH=14, 0.1 g/mL Fe$_3$O$_4$, 25 °C, 12 h) had a content of about 3.16%, 1.641%, 22.843%, 0% and 0.392% respectively, indicating that there were organic compounds on the solid product.

Table S5 TOC content of solid products with different reaction conditions

	(pH=14, 0.1 g/mL Fe$_3$O$_4$, 25 °C, 12 h)	(pH=14, 0 g/mL Fe$_3$O$_4$, 80 °C,12 h)	(pH=14, 0.1 g/mL Fe$_3$O$_4$, 80 °C, 12 h)
TOC (g/kg)	5.77	8.83	1.83

Table S5 displayed TOC content of solid products generated by different reaction conditions. When the reaction condition was pH=14, 0.1 g/mL Fe$_3$O$_4$, 25 °C, 12 h, the TOC content of the solid product was 5.77 g/kg. When the reaction condition was pH=14, 0 g/mL Fe$_3$O$_4$, 80 °C,12 h, the TOC content of the solid product was 8.33 g/kg. In the reaction condition of pH=14, 0.1 g/mL Fe$_3$O$_4$, 80 °C, 12 h, the TOC content of the solid product was 1.83 g/kg.

Table S6 Comparison of removal efficiency of different processes on spent electroless nickel plating solution (SENPS)

Method	SENPS		Removal efficiency	
	Nickel Species	Concentration	Nickel	TOC
Sulfide precipitation[1]	Ni^{2+}	100 mg/L	94%	-
Sulfide precipitation[2]	Ni^{2+}	100 mg/L	99%	-
Photo-Fenton[3]	Ni^{2+}	250 mg/L	90.4%	-
Ion exchange -PEC-Chemical precipitation[4]	Ni^{2+}	28000 mg/L	78%	-
Extraction[5]	Ni^{2+}	500 mg/L	90%	-
Biosorption[6]	Ni^{2+}	46.82 mg/L	40%	-
Fe(III)/UV/NaOH[7]	Ni(II)-citrate	168 mg/L	58%	58%
Fenton-like method-precipitation[8]	Ni(II)-citrate	350 mg/L	99.9%	58.5%(COD)
Adsorption (CES)[9]	Ni(II)-citrate	283 mg/ L	87%	66%
Electrochemical advanced oxidation processes[10]	Ni-EDTA	350 mg/L	90%	30%
Chelate extraction[11]	Ni(II)-EDTA	7.26 mg/L	99.13%	-
Alkaline Fe_3O_4 hydrothermal process (This work)	Nickel Lactate Ni(II)-EDTA	12448.8 mg/L	99.99%	81%

The removal efficiency of different treatment processes on spent electroless nickel plating solution was compared and listed in **Table S6**. By comparison, the removal efficiency of nickel of this process on organic complexed nickel could reach 99.99%, and the removal efficiency of TOC was as high as 81%, better than that of similar process reported in the literatures.

Table S7 Stability constant of Ni(II) complex species (K_f)

Species	Log K
$Ni(OH)^+$	-9.90
$Ni(OH)_2$ (aq)	-18.99
$Ni(OH)_3^-$	-29.99
NiH_2EDTA (aq)	24.74
$NiEDTA^{2-}$	20.11
$NiHEDTA^-$	23.64
$NiOHEDTA^{3-}$	7.56

Table S7 listed part of nickel complex species and their stability constant (K_f).

Table S8 Pharmaceutical cost account

Chemicals	Dosage	Price	Cost
Fe_3O_4	100 kg/m^3	447.66 USD/m^3	44.77 USD/m^3
NaOH	100 kg/m^3	279.79 USD/m^3	27.98 USD/m^3
Total	-	-	72.75 USD/m^3

Table S8 showed the pharmaceutical cost of the treatment process when treating about 1 m^3 spent electroless nickel plating solution. By calculation, the pharmaceutical cost was 72.75 USD/m^3.

Table S9 Mossbauer parameter of the solid product (pH=14, 0.1 g/mL Fe_3O_4, 80 °C, 12 h)

	Site	Is(mm/s)	Qs(mm/s)	H(T)	Γ(mm/s)	Area(%)
$NiFe_2O_4$	A	0.25	-0.04	51.35	0.51	22.0
	B	0.23	0.02	49.03	0.54	37.8
Fe_3O_4	A	0.50	-0.03	46.00	0.55	25.4
	B	0.57	0.05	42.44	0.82	12.0
SP- $NiFe_2O_4$		0.19	0.61	-	0.49	2.8

Table S9 listed the electronic and magnetic Mössbauer parameters corresponding to the curves exhibited in **Fig. 8a**, including chemical shift, quadrupole splitting, ultrafine field, and relative area of Fe^{3+} at different sites.
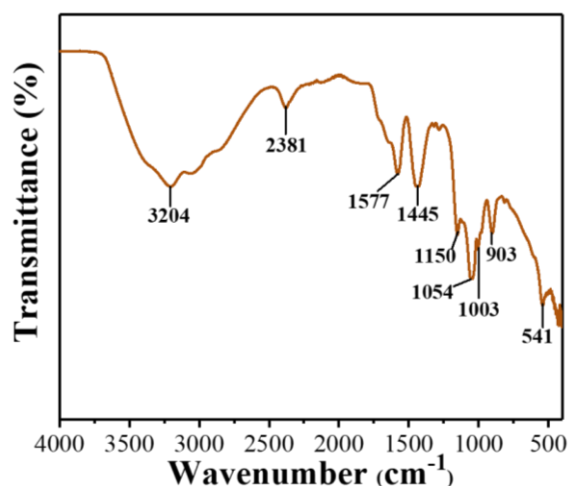
Fig. S1 ATR-FTIR curve of spent electroless nickel plating solution

ATR-FTIR curve of spent electroless nickel plating solution was shown in **Fig. S1**, which the peak at 3204 cm^{-1} corresponded to the stretching vibration of -OH, and the peak at 2381 cm^{-1} was related to O=C=O[12]. There was no response vibration of C-O in the corresponding carboxylic acid at 1700~1750 cm^{-1}, but appeared at 1577 cm^{-1}, causing by the coordination of carboxyl groups in carboxylic acid with metal ions (Ni^{2+})[13]. The peak at 1445 cm^{-1} belonged to C=O[14]. The signal of 1150 cm^{-1} was considered as the bending vibration of Ni^{2+} and organic acid coordination[15]. The peak at 1054 cm^{-1} belonged to the stretching vibration of N-H bond[16].
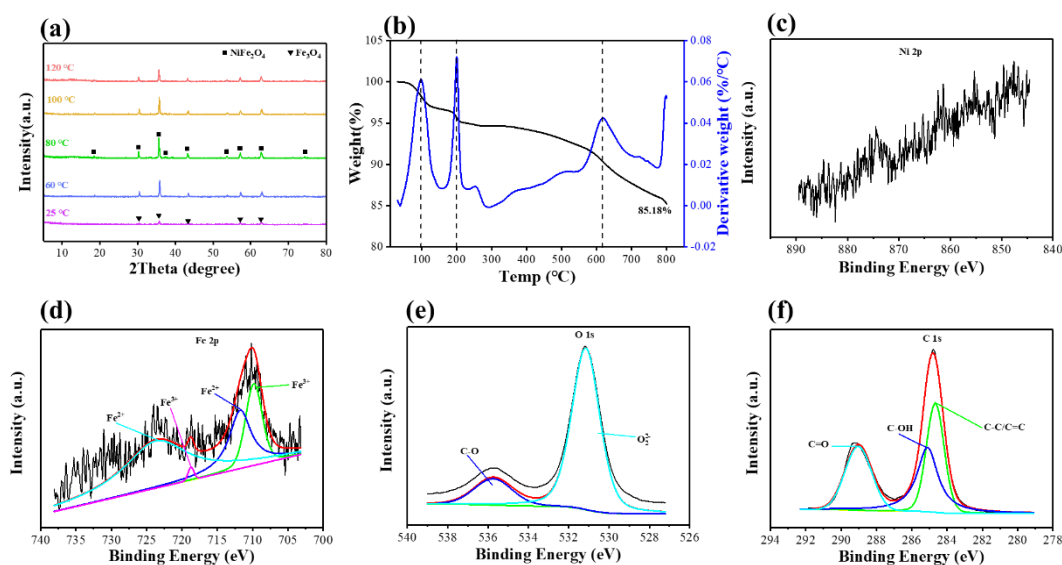
Fig. S2 (a) XRD patterns of solid products with different temperature (pH =14, 0.1 g/mL Fe_3O_4, 12 h), (b-f) TG-DTG curves and XPS spectra of solid product (pH=14, 0.1 g/mL Fe_3O_4, 25 °C, 12 h), which (c) Ni 2p, (d) Fe 2p, (e) O 1s and (f) C 1s

XRD spectrum of solid products with different temperature was displayed in **Fig. S2a**, indicating that $NiFe_2O_4$ phase could be formed at a certain temperature (60~120 °C). However, at 25 °C, only Fe_3O_4 phase was observed, which was considered that nickel in the product still existed in the form of organic nickel.

Subsequently, TG-DTG and XPS were carried out to analyze the solid product generated at the following conditions: pH=14, 0.1 g/mL Fe_3O_4, 25 °C, 12 h.TG-DTG curves of the solid product was shown in **Fig. S2b**. It could be seen that the change between 100~200 °C belonged to the loss of adsorbed water and crystal water in the product while the change of 600 ~800 °C was caused by the degradation of organic compounds.

XPS spectra were exhibited in **Fig. S2c-f**. In Ni 2p spectrum, no obvious bond energy peak was found (**Fig. S2c**), which was considered that organic complexed nickel was not broken completely and attached to the surface of Fe_3O_4.However, in Fe 2p spectrum (**Fig. S2d**), the XPS peaks at 711.0 and 709.0 eV could be detected obviously, which belonged to Fe^{3+} and Fe^{2+} in Fe_3O_4 respectively[17]. In the XPS spectrum of O 1s (**Fig. S2e**), the peak at 535.8 eV belonged to C-O[18]. The peaks at 284.5 eV, 285.2 eV and 289.0 eV appeared in the XPS spectrum of C 1s (**Fig. S2f**) were related to C-C/C=C,

C-OH and C=O, respectively[19]. To sum up, organic impurities (Formula $C_xH_yO_z$) might exist on the surface of solid product generated at the following reaction conditions: pH=14, 0.1 g/mL Fe_3O_4, 25 °C, 12 h.
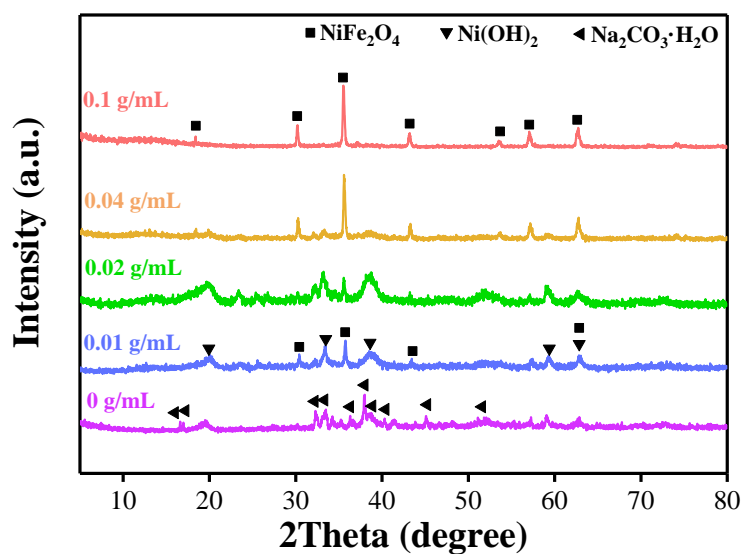
Fig. S3 XRD patterns of solid product of the hydrothermal reaction with different Fe_3O_4 dosage

Fig. S3 showed XRD patterns of solid product of the hydrothermal reaction with different Fe_3O_4 dosage. When no Fe_3O_4 was used in the hydrothermal reaction, the solid product consisted of $Na_2CO_3 \cdot H_2O$ and amorphous organic nickel complex. When the Fe_3O_4 dosage was 0.01 or 0.02 g/mL, the primary phases in the solid products were $Ni(OH)_2$ (PDF 00-001-1047) and $NiFe_2O_4$ (PDF 01-074-2081) with low crystallinity. As the Fe_3O_4 dosage gradually increased, the $Ni(OH)_2$ phase diminished while the $NiFe_2O_4$ phase increased, and the crystallinity also steadily improved. When the Fe_3O_4 dosage was 0.1 g/mL, the predominant phase in the solid product was $NiFe_2O_4$.
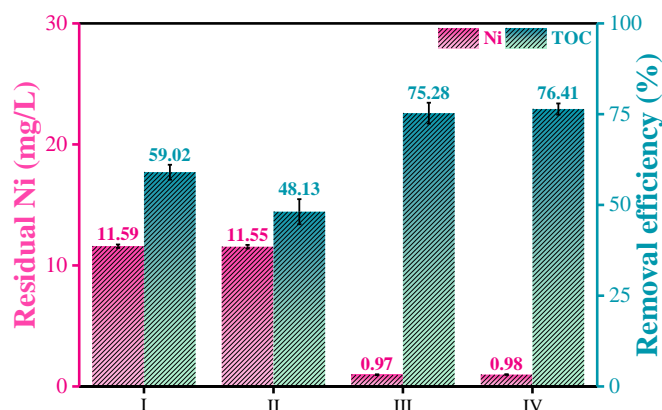
Fig. S4 Residual nickel concentration and removal efficiency of TOC with different reaction conditions, which I:80 ℃, 0 g/mL Fe_3O_4, pH > 14, 12 h, II: 80 ℃, 0 g/mL Fe_3O_4, pH = 14, 12 h, III: 80 ℃, 0.1 g/mL Fe_3O_4, pH > 14, 12 h, IV: 80 ℃, 0.1 g/mL Fe_3O_4, pH = 14, 12 h

Fig. S4 showed residual nickel concentration and removal efficiency of TOC under different reaction conditions. When reaction conditions were 80 ℃, 0 g/mL Fe_3O_4, pH > 14, 12 h, residual nickel was 11.59 mg/L and removal efficiency of TOC was 59.02% (column I). When reaction conditions were 80 ℃, 0 g/mL Fe_3O_4, pH = 14, 12 h, residual nickel concentration was 11.55 mg/L and removal efficiency of TOC was 48.13% (column II). When reaction conditions were 80 ℃, 0.1 g/mL Fe_3O_4, pH > 14, 12 h, residual nickel was 0.97 mg/L and removal efficiency of TOC was 75.28% (column III). When reaction conditions were 80 ℃, 0.1 g/mL Fe_3O_4, pH = 14, 12 h, residual nickel was 0.98 mg/L and removal efficiency of TOC was 76.41% (column IV).

Compared column I and II (or III and IV), it could not get a better removal efficiency by increasing alkaline concentration alone. Besides, the removal efficiency of TOC can only reach 59.02% and 48.13%., indicating that organics was not broken and degraded but was removed from aqueous phase to solid phase which became solid pollutant (see **Fig. S3** purple line, the phase of solid product treated by alkaline alone was $Ni(OH)_2$ and organic complexes).

Compared column I and III (or II and IV), when Fe_3O_4 added, the removal efficiency of nickel and TOC could be improved, indicating that the addition of Fe_3O_4

was to degrade the organic complexes by producing reactive oxygen species and convert nickel complexes to $NiFe_2O_4$ as a valuable nano-material (see **Fig. S3** red line, the phase was $NiFe_2O_4$ and Fe_3O_4).
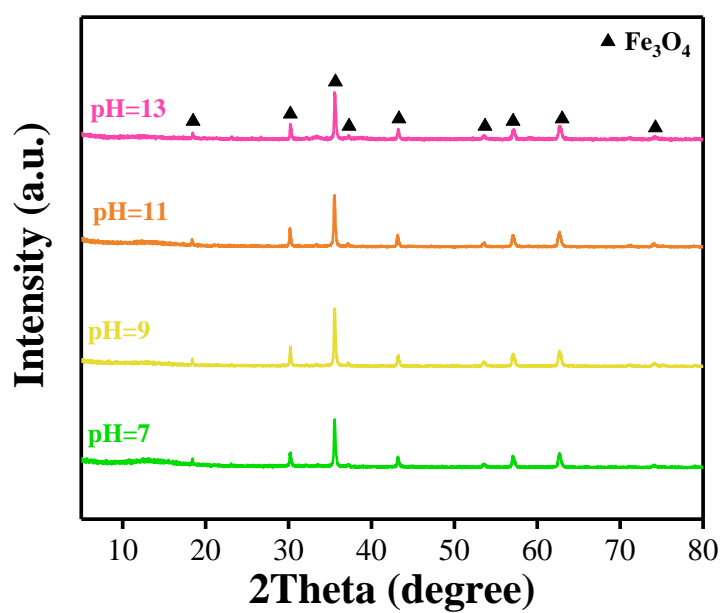
Fig. S5 XRD patterns of solid product of the hydrothermal treatment with different pH value of the solution

XRD patterns of solid product of the hydrothermal treatment with different pH value of the solution were shown in **Fig. S5**. It could be seen that the product obtained at pH < 13 consisted mainly of an amorphous phase and the Fe_3O_4 phase, $NiFe_2O_4$ phase was not formed.
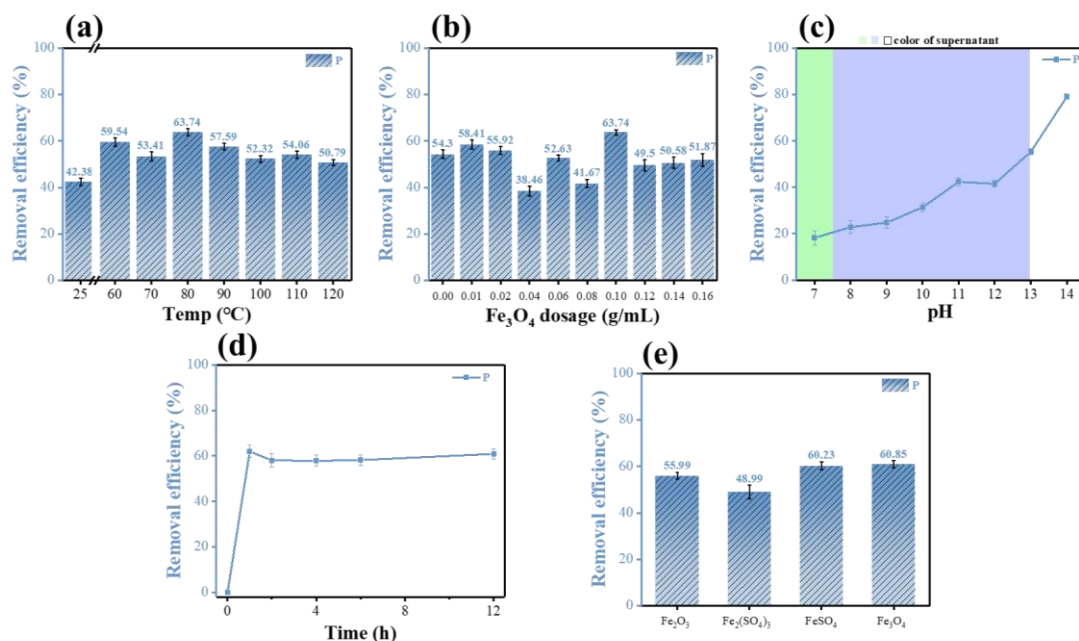
Fig. S6 Removal efficiency of phosphorus via hydrothermal treatment process in an alkaline environment containing Fe_3O_4, (a) temperature (pH =14, 0.1 g/mL Fe_3O_4, 12 h), (b) Fe_3O_4 dosage (pH=14, 80 ℃, 12 h), (c) pH value of the solution (0.1 g/mL Fe_3O_4, 80 ℃, 12 h), (d) reaction time (pH =14, 0.1 g/mL Fe_3O_4, 80 ℃), (e) iron reagents (pH =14, 0.1 g/mL iron reagents, 80 ℃, 12 h)

The effect of temperature, Fe_3O_4 dosage, pH value of the solution, reaction time and iron reagents on the removal of phosphorus were respectively shown in **Fig. S6**. It could be seen from **Fig. S6a** that the removal efficiency of phosphorus was 63.74% at 80 ℃. In **Fig. S6b**, when Fe_3O_4 dosage was 0.1 g/mL, the removal efficiency of phosphorus was 63.74%. **Fig. S6c** showed that the removal efficiency of phosphorus increased with the increase of pH value and reached 79% when pH=14. **Fig. S6d** reflected that about 63% of phosphorus could be removed at 1 h, and the removal efficiency did not change significantly with the extension of time. **Fig. S6e** displayed that the addition of Fe_2O_3, $Fe_2(SO_4)_3$, $FeSO_4$ or Fe_3O_4 to the hydrothermal reaction gave a removal efficiency of phosphorus of 55.99%, 48.99%, 60.23% and 60.85%, respectively.
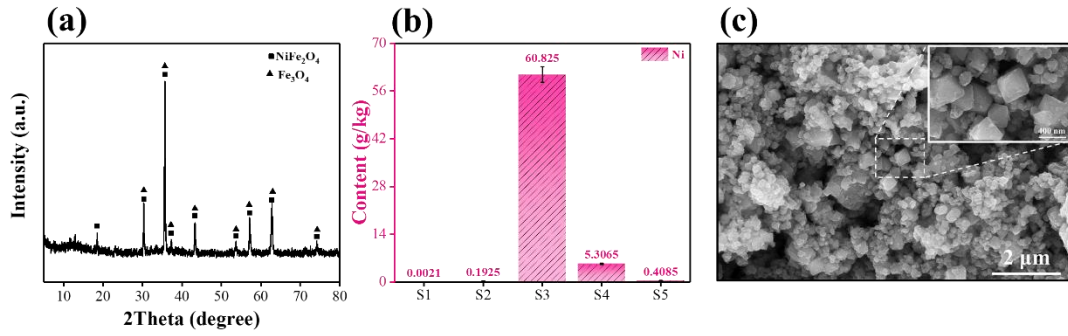
Fig. S7 (a) XRD pattern, (b) concentration of nickel of different speciation and (c) SEM image of the solid product

XRD pattern of the solid product was shown in **Fig. S7a** generated at the following environment:80 ℃, 0.1 g/mL Fe_3O_4, pH=14, 12 h, which indicated that the precipitated phases were mainly nickel ferrite （$NiFe_2O_4$）and Fe_3O_4. **Fig. S7b** exhibited the concentration of different forms of nickel in the solid product via Tessier's five-step extraction method, which the total content of nickel was about 66.7346 g/kg. Step 3 represented the content of nickel in the ferrite-bound state which had a content of 60.825 g/kg. SEM image of the solid product in **Fig. S7c** revealed that the solid product had obvious spinel structure. It was considered that nickel in the solid product mainly existed in the form of ferrite-bound state. The recovery efficiency of nickel was 97.75% with the following calculation:

$$\text{Efficiency}(\%) = \frac{m_{Ni(NiFe_2O_4)}}{m_{Ni(SENPS)}} = \frac{60.825 \; g/kg}{12448.8 \; mg/L \times 5 \; mL} = 97.75\%$$
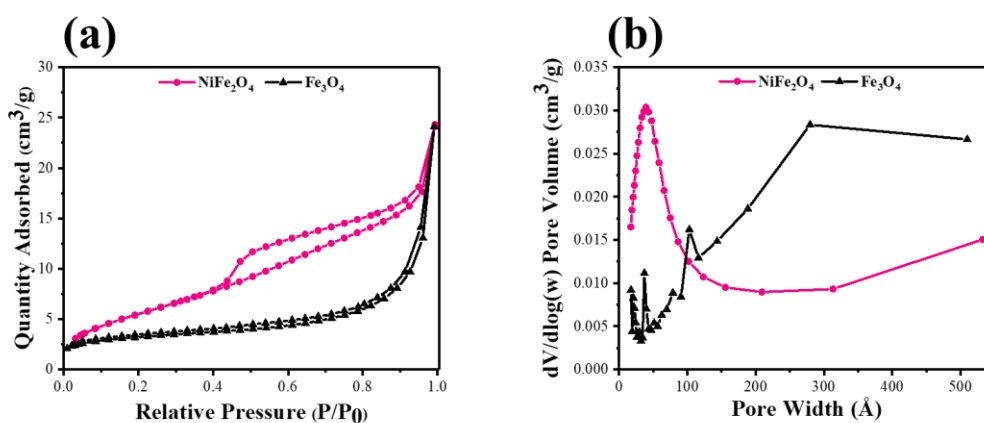
Fig. S8 (a) N_2 adsorption-desorption curve and (b) pore size distribution curve of

Fe_3O_4 and solid product $NiFe_2O_4$

The N_2 adsorption-desorption experiment showed the structural characteristic of the solid sample $NiFe_2O_4$ and Fe_3O_4 (**Fig. S8**). In **Fig. S8a**, the isotherms of the materials above could be classified as type IV, which was the characteristic of porous materials. The BET specific surface area of solid sample $NiFe_2O_4$ was about 21.4457 m^2/g, larger than that of Fe_3O_4(10.7195 m^2/g). Besides, from the pore size distribution curve (**Fig. S8b**), samples contained mesoporous (2~50 nm) and microporous (> 50 nm)[20], which solid sample $NiFe_2O_4$ was mainly mesoporous while Fe_3O_4 was mainly microporous.
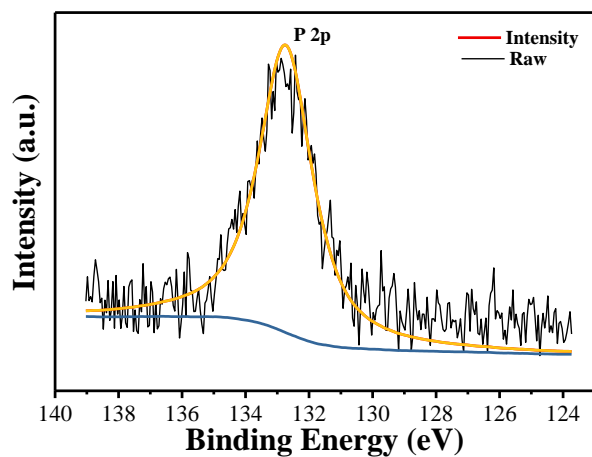
Fig. S9 XPS spectrum of the solid product (P 2p)

It could be seen in the P 2p spectrum (**Fig. S9**) of the solid product generated at the following conditions (80 °C, 0.1 g/mL Fe_3O_4, pH=14, 12 h) that the peak appeared at 132.8 eV was related to P (+5) [21], indicating that phosphorus existed on the surface of the solid product.
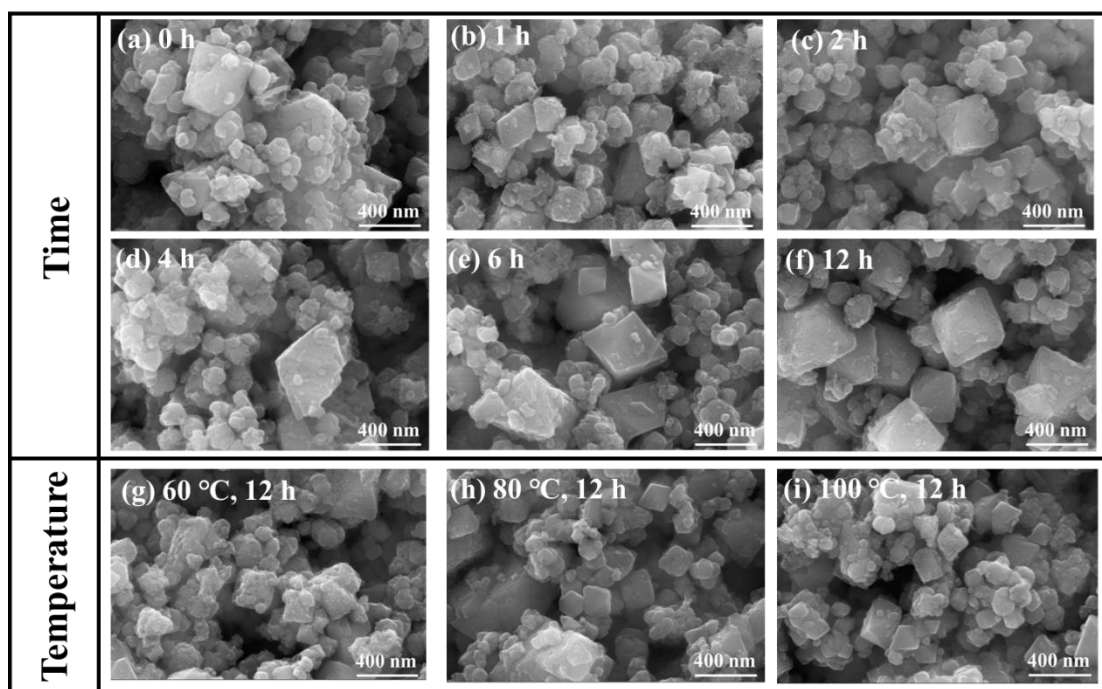
Fig. S10 SEM images of the solid products in different reaction time (a-f) and different temperature (g-i)

The evolution of the product's crystal phase structure during the reaction was observed by SEM (**Fig. S10a-f**). The Fe_3O_4 reagent was mostly amorphous spherical particles with an uneven surface. After 1 h, although the nickel removal rate exceeded 99.99%, there was still no clearly identifiable spinel-shaped nickel ferrite structure in the product. The spinel morphology gradually appeared as the reaction advanced (2–12 h), which corresponded to the entrance of nickel into the Fe_3O_4 lattice and the transformation to generate $NiFe_2O_4$. Many spinel-shaped particles that were approximately 400 nm in size could be seen in the SEM image from the product after the reaction had been carried out for 12 h. In addition, the crystal surface of the solid product became smoother with rising hydrothermal temperature (**Fig. S10g-i**). That is, running the hydrothermal reaction at a suitable temperature for enough time was beneficial to the crystal growth
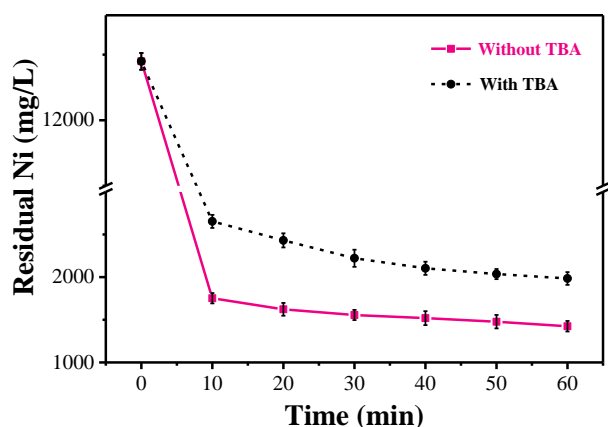
Fig. S11 Residual nickel concentration in supernatant by effect of TBA as hydroxyl radical scavenger (pH=12.5, 0.1 g/mL Fe_3O_4, 25 °C)

In order to determine whether hydroxyl radical (·OH) was involved in the degradation and removal of the organic nickel complex, the EPR experiment containing tert-butanol (TBA)-a typical ·OH quencher was carried out (to facilitate the observation and sampling, the reaction was carried out with 0.1 g/mL Fe_3O_4 at pH = 12.5 and 25 °C).The results in **Fig. S11** indicated that the concentration of residual nickel increased with the presence of TBA, suggesting that ·OH was involved in the degradation of the organic nickel complex.
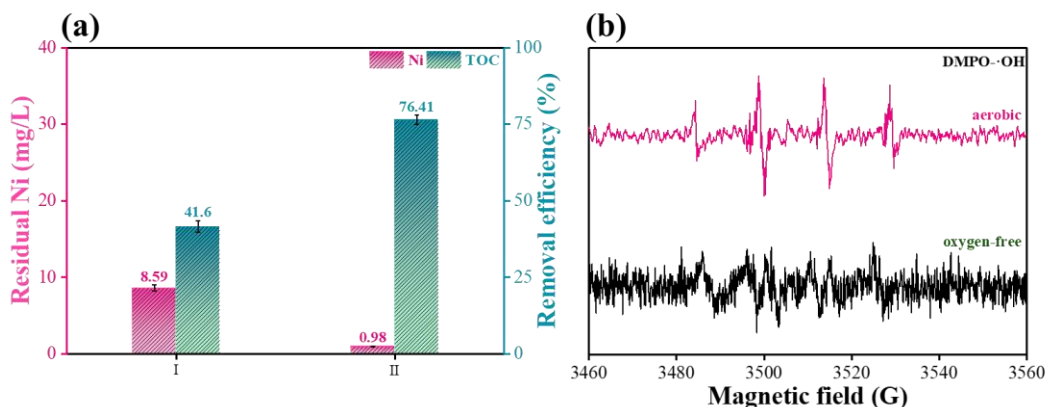
Fig. S12 (a) Residual nickel concentration and removal efficiency of TOC with different reaction conditions, which I: oxygen-free, II: aerobic (80 ℃, 0.1 g/mL Fe_3O_4, pH = 14, 12 h) and (b) EPR spectrum of oxygen-free and aerobic conditions

    Fig. S12a exhibited the residual nickel and TOC removal efficiency in the conditions of oxygen-free or aerobic. When oxygen-free, residual nickel was 8.59 mg/L and removal efficiency of TOC was 41.6% (column I), while in aerobic condition, the residual nickel was 0.98 mg/L and removal efficiency of TOC was 76.41% (column II). The results indicated that in oxygen-free conditions, the removal efficiency of TOC was weaker than that of aerobic, nickel decrease was due to the effect of alkaline conditions. EPR spectrum (**Fig. S12b**) showed the DMPO-·OH signals of oxygen-free, but weaker than that of aerobic, indicating that besides dissolved oxygen, there might be other oxygen groups participated in the production of hydroxyl radicals [22, 23].
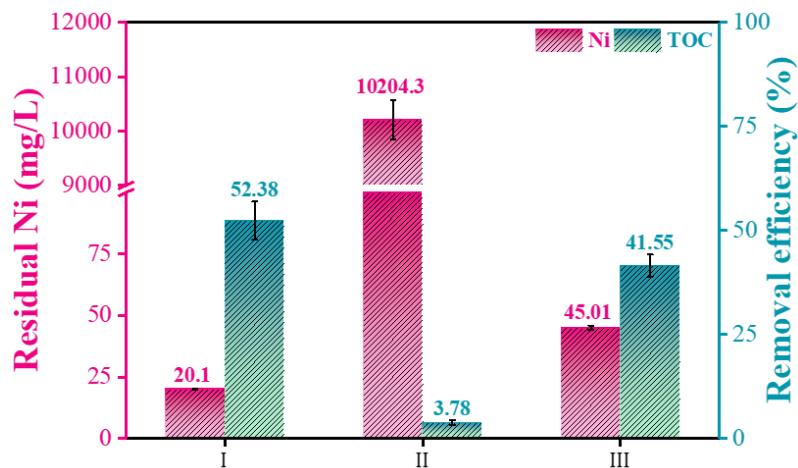
Fig. S13 Residual nickel concentration and removal efficiency of TOC with different reaction conditions, which I: 25 °C, 0.1 g/mL Fe_3O_4, pH = 14, 12 h, II: 25 °C, 0.1 g/mL Fe_3O_4, equivalent H_2O, 12 h, III: 25 °C, 0 g/mL Fe_3O_4, pH = 14, 12 h

Fig. S13 exhibited residual nickel concentration and removal efficiency of TOC with different reaction conditions. When reaction was conducting at the following conditions: 25 °C, 0.1 g/mL Fe_3O_4, pH = 14, 12 h, the residual nickel was 20.1 mg/L and removal efficiency of TOC was 52.38% (column I). When reacting under the conditions of 25 °C, 0.1 g/mL Fe_3O_4, equivalent H_2O, 12 h, residual nickel was about 10204.3 mg/L and removal efficiency of TOC was 3.78% (column II). When reaction conditions were 25 °C, 0 g/mL Fe_3O_4, pH = 14, 12 h, residual nickel was 45.01 mg/L and removal efficiency of TOC was 41.55% (column III).

The comparison between column I and column II indicated that the alkaline environment not only affected the stability of the complex structure, but also had the ability to disrupt the complex structure. Compared column I and III, it indicated that the addition of Fe_3O_4 was to further degrade the complexes by producing active oxygen radicals.
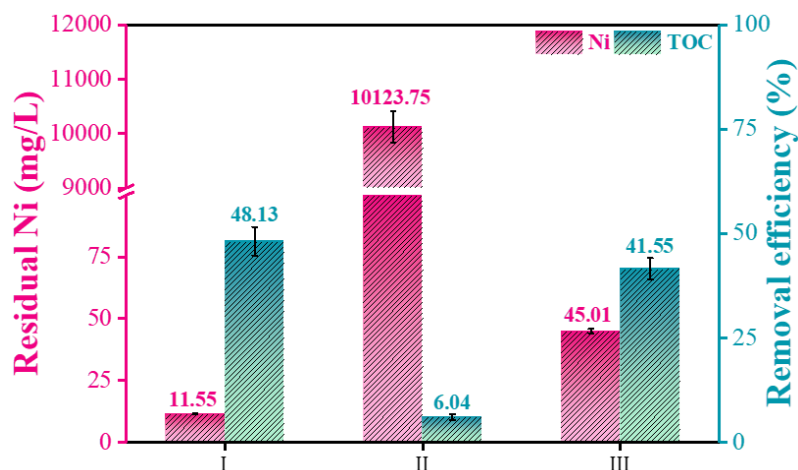
23

Fig. S14 Residual nickel concentration and removal efficiency of TOC with different reaction conditions, which I: 80 °C, 0 g/mL Fe_3O_4, pH = 14, 12 h, II: 80 °C, 0 g/mL Fe_3O_4, equivalent H_2O, 12 h, III: 25 °C, 0 g/mL Fe_3O_4, pH = 14, 12 h

Fig. S14 exhibited residual nickel concentration and removal efficiency of TOC with different reaction conditions. When reaction was conducting at the following conditions: 80 °C, 0 g/mL Fe_3O_4, pH = 14, 12 h, the residual nickel was 11.55 mg/L and removal efficiency of TOC was 48.13% (column I). When reacting under the conditions of 80 °C, 0 g/mL Fe_3O_4, equivalent H_2O, 12 h, residual nickel was about 10123.75 mg/L and removal efficiency of TOC was 6.04% (column II). When reaction conditions were 25 °C, 0 g/mL Fe_3O_4, pH = 14, 12 h, residual nickel was 45.01 mg/L and removal efficiency of TOC was 41.55% (column III).

The differences between column I and II was caused by the effect of alkaline conditions. The invasion of OH^- would influence the structure of nickel complexes and weakened their stability. Besides, strong alkalis had ability of breaking complex network structure. The comparison between column I and III showed that appropriate temperature conditions would have a role in the removal of nickel complexes.

Reference

1. S. Jerroumi, M. Amarine, H. Nour, B. Lekhlif and J. E. Jamal, *Water Qual. Res. J. Can.*, 2020, **55**, 345-357.

2. N. Mihara, K. Soya, D. Kuchar, T. Fukuta and H. Matsuda, *GLOBAL NEST J.*, 2008, **10**, 101-107.

3. E.-C. Su, B.-S. Huang and M.-Y. Wey, *RSC Adv.*, 2016, **6**, 71273-71281.

4. J. Zhang, R. Djellabi, S. Zhao, M. Qiao, F. Jiang, M. Yan and X. Zhao, *J. Hazard. Mater.*, 2020, **394**, 122559.

5. R. N. R. Sulaiman and N. Othman, *J. Environ. Chem. Eng.*, 2018, **6**, 1814-1820.

6. C. E. R. Barquilha, E. S. Cossich, C. R. G. Tavares and E. A. Da Silva, *J. Water Process Eng.*, 2019, **32**, 100904.

7. Z. Jiang, Y. Ye, X. Zhang and B. Pan, *Chemosphere*, 2019, **234**, 917-924.

8. H. Liang, K. Xiao, L. Wei, B. Yang, G. Yu, S. Deng, H. Duan, C. Zhu, J. Li and J. Zhang, *J. Hazard. Mater.*, 2019, **374**, 167-176.

9. G. Peng, S. Deng, F. Liu, C. Qi, L. Tao, T. Li and G. Yu, *J. Clean. Prod.*, 2020, **262**, 121416.

10. H. Rong, C. Zhang, Y. Sun, L. Wu, B. Lian, Y. Wang, Y. Chen, Y. Tu and T. D. Waite, *Chem. Eng. J.*, 2022, **431**, 133230.

11. P. Yan, M. Ye, S. Sun, X. Xiao, W. Dai and N. Zhang, *J. Clean. Prod.*, 2016, **122**, 308-314.

12. M. Haurat, T. Tassaing and M. Dumon, *J. Supercrit. Fluid.*, 2022, **182**, 105534.

13. R. Lin, L. Ge, H. Diao, V. Rudolph and Z. H. Zhu, *ACS Appl. Mater. Interfaces*, 2016, **8**, 32041-32049.

14. Q. Lan, C. Liu, F. Yang, S. Liu, J. Xu and D. Sun, *J. Colloid. Interface Sci.*, 2007, **310**, 260-269.

15. R. Darvishi, M. Darvishi and A. Moshkriz, *Int. J. Polym. Sci.*, 2021, **2021**, 1-22.

16. P. Song, C. Sun, J. Wang, S. Ai, S. Dong, J. Sun and S. Sun, *Chemosphere*, 2022, **287**, 131971.

17. P. B. Liu, Y. Huang and X. Sun, *Mater. Lett.*, 2013, **112**, 117-120.

18. S. R. Teeparthi, E. W. Awin and R. Kumar, *Sci. Rep.*, 2018, **8**, 5541.

19. X. Jiang, W. Yan, Z. L. Xiong and L. S. Zhao, *Environ. Sci.: Nano*, 2022, **9**, 2939-2953.

20. H. Yi, L. Cui, X. Q. Huo, L. Qin, Y. K. Fu, S. Y. Liu, L. Li, M. M. Zhang, M. Chen and G. M. Zeng, *Environ. Sci.: Nano*, 2022, **9**, 815-826.

21. T. Fu, J. T. Fan, Y. G. Shen and J. M. Sun, *Mater. Chem. Phys.*, 2017, **189**, 105-110.

22. A. D. Bokare and W. Choi, *J. Hazard. Mater.*, 2014, **275**, 121-135.

23. H. Cai, X. Li, D. Ma, Q. Feng, D. Wang, Z. Liu, X. Wei, K. Chen, H. Lin, S. Qin and F. Lu, *Sci. Total Environ.*, 2021, **764**, 144200.